Atomistic simulation for the phase stability and site preference of $R_3(Fe,T)_{29}$ (R = Nd,Gd,Y; T = Ta,W)

2005 J. Phys.: Condens. Matter 17 1351

(http://iopscience.iop.org/0953-8984/17/8/014)

INSTITUTE OF PHYSICS PUBLISHING JOURNAL OF PHYSICS: CONDENSED MATTER

J. Phys.: Condens. Matter **17** (2005) 1351–1362 doi:10.1088/0953-8984/17/8/014

Atomistic simulation for the phase stability and site preference of $R_3(Fe, T)_{29}$ (R = Nd, Gd, Y; T = Ta, W)

Lin Jia[1], **Jiang Shen**[1] **and Nan-Xian Chen**[1,2]

[1] Institute of Applied Physics, University of Science and Technology Beijing, Beijing 100083, People's Republic of China
[2] Department of Physics, Tsinghua University, Beijing 100084, People's Republic of China

E-mail: jlin@aphy.iphy.ac.cn

Received 8 July 2004, in final form 24 January 2005
Published 11 February 2005
Online at stacks.iop.org/JPhysCM/17/1351

Abstract

The phase stability and site preference of the intermetallics $R_3(Fe, T)_{29}$ (R = Nd, Gd, Y; T = Ta, W) with $Nd_3(Fe, Ti)_{29}$ structure have been investigated by lattice inversion potentials. The calculated results indicate that each of the stabilizing elements Ta and W significantly decreases the cohesive energy of $R_3(Fe, T)_{29}$ and plays a role in stabilizing the 3:29 structure. Among the 11 different kinds of Fe sites in these compounds the preferential sites of Ta and W are $4i_3$, $4i_4$ and 4g sites. The calculated lattice parameters of $R_3(Fe, T)_{29}$ compounds are in good agreement with the experimental data. The structural stability of the $R_3(Fe, T)_{29}$ compounds is further tested at different temperatures. Based on the pair potential curves an intuitive explanation for the phase stability and solubility is made.

1. Introduction

The rare earth (R)–transition metal (T) intermetallic compounds have attracted great interest because of their potential application for permanent magnets [1]. In 1992, Collocott *et al* [2] synthesized a new compound defined as $Nd_2(Fe, Ti)_{19}$. Subsequently, x-ray powder diffraction [3] and neutron diffraction [4] showed that this new ternary compound crystallizes in monoclinic structure with space group $P2_1/c$ and the exact formula is $Nd_3(Fe, Ti)_{29}$. Later, Kalogirou *et al* [5] suggested that $Nd_3(Fe, Ti)_{29}$ could be described more accurately in the $A2/m$ space group with 13 different crystallographic sites, including 11 positions for transition metal atoms and two positions for rare-earth atoms. From then on, many intermetallic compounds $R_3(Fe, T)_{29}$ (R = rare earth and Y, T = Ti, V, Cr, Mn, Mo) with $Nd_3(Fe, Ti)_{29}$-type structure have been synthesized [6–8].

In our previous work, we have studied the phase stability and site preference of $R_3(Fe, T)_{29}$, in which T represents some certain 3d and 4d elements; the results are in good agreement with

experimental results. In this work, we expand the pair potential method to the $R_3(Fe, T)_{29}$ compounds with T = 5d elements (Ta, W).

An introduction to the methodology for the calculation is given in section 2; the results for a variety of structural calculations are shown in section 3; in section 4 discussion and analysis are presented and in the last section conclusions are summarized.

2. Methodology

2.1. Lattice inversion technique

Here, we take a single element crystal as an example to explain how to use Chen's lattice inversion method to obtain the interatomic pair potentials [9–13]. The crystal cohesive energy can be written as

$$E(x) = \tfrac{1}{2}\sum_{n=1}^{\infty} r_0(n)\phi(b_0(n)x) \tag{1}$$

where x is the nearest-neighbour interatomic distance, $r_0(n)$ the nth-neighbour coordination number, $b_0(n)x$ the distance between the reference central atom and its nth neighbour and $\Phi(x)$ the pair potential. By a self-multiplicative process of the element in $\{b_0(n)\}$, $\{b(n)\}$ forms a closed multiplicative semi-group. Then the general equation for the interatomic pair potential obtained from inversion can be expressed as

$$\phi(x) = 2\sum_{n=1}^{\infty} I(n)E(b(n)x). \tag{2}$$

The coefficient $I(n)$ can be obtained by

$$\sum_{b(n)/b(k)} I(n)r\left(b^{-1}\left[\frac{b(k)}{b(n)}\right]\right) = \delta_{k1}. \tag{3}$$

They are uniquely determined by the crystal geometrical structure, which is independent of the kind of specific element. Thus the interatomic pair potentials can be obtained from the known cohesive energy function $E(x)$.

2.2. Acquisition of effective potentials

Due to the structural complexity of ternary alloys $R_3(Fe, T)_{29}$, the *ab initio* calculation of the cohesive energy curves for $R_3(Fe, T)_{29}$ is impossible or very difficult. In order to find some effective interatomic potentials with the lattice inversion technique, a practical method of performing the calculation of cohesive curve is needed. For this, the search and design of some simple and virtual structures covering the necessary interatomic potentials are important for us. For example, in order to obtain potentials $\Phi_{R-R}(r)$, $\Phi_{Fe-Fe}(r)$ and $\Phi_{R-Fe}(r)$, we designed three structures as follows.

First, let us consider the structure of BCC Fe as a B_2 or CsCl structure with two simple cubic sublattices Fe_1 and Fe_2. Thus, we calculate

$$\begin{aligned} E(x) &= E_{Fe}^{BCC}(x) - E_{Fe_1}^{SC}(x) - E_{Fe_2}^{SC}(x) \\ &= \sum_{i,j,k\neq 0}^{\infty} \Phi_{Fe-Fe}\left(\sqrt{\tfrac{4}{3}[(i-\tfrac{1}{2})^2 + (j-\tfrac{1}{2})^2 + (k-\tfrac{1}{2})^2]}x\right) \end{aligned}$$

where x is the nearest-neighbour distance in the BCC structure, $E_{Fe}^{BCC}(x)$ represents the total energy curve with a BCC structure and $E_{Fe_1}^{SC}(x)$ or $E_{Fe_2}^{SC}(x)$ is the total energy function with

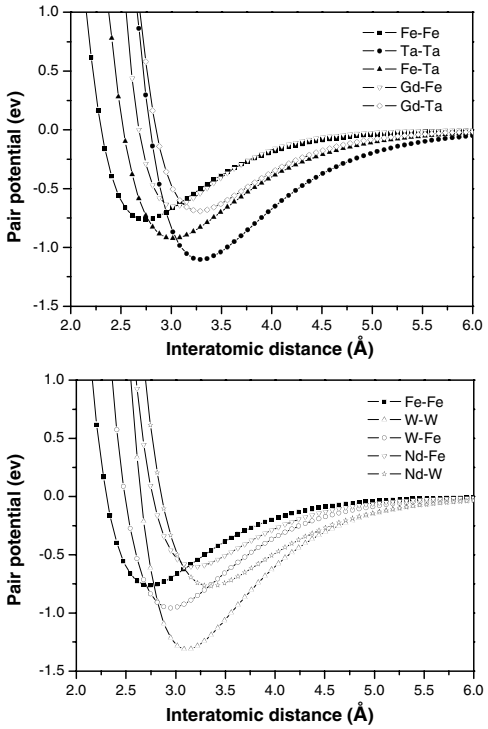

Figure 1. Some important interatomic potentials for R–Fe–T (R = Gd, Nd; T = Ta, W) compounds.

a simple cubic structure. Now, $E(x)$ automatically becomes the cohesive energy function of one Fe_1 atom with all the Fe_2 atoms. Then the $\Phi_{Fe-Fe}(r)$ can be obtained directly by using the lattice inversion technique.

Similarly, let us consider a metal R with the FCC structure. We may calculate

$$E(x) = E_R^{FCC}(x) - E_R^{SC}(x) - E'_R(x)$$

where $E_R^{SC}(x)$ is attributed to the simple cubic structure, in which all the atoms occupy the corner sites and $E'_R(x)$ is attributed to the atoms occupying the face centre sites. Thus, the $\Phi_{R-R}(x)$ can also be obtained by the lattice inversion technique.

The calculation of the total energy curve related to $\Phi_{R-Fe}(x)$ is very hard to perform. We find that the calculation for R_3Fe with $L1_2$ structure can be done in a nearly equilibrium position, and this gives simply the three parameters for the cohesion function under the Morse approximation or Rose approximation. From the above procedures the interatomic potentials can be obtained. Several important relevant interatomic pair potential curves are shown in figure 1.

2.3. Application of the pair potentials

Chen's inversion theorem has been developed to a rigorous and concise approach to obtain the interatomic pair potentials based on the cohesive energy curves. We have made a serial application of the interatomic pair potentials to observe the consistency between the calculated and experimental results. It has been applied successfully to study the lattice dynamics [14, 15],

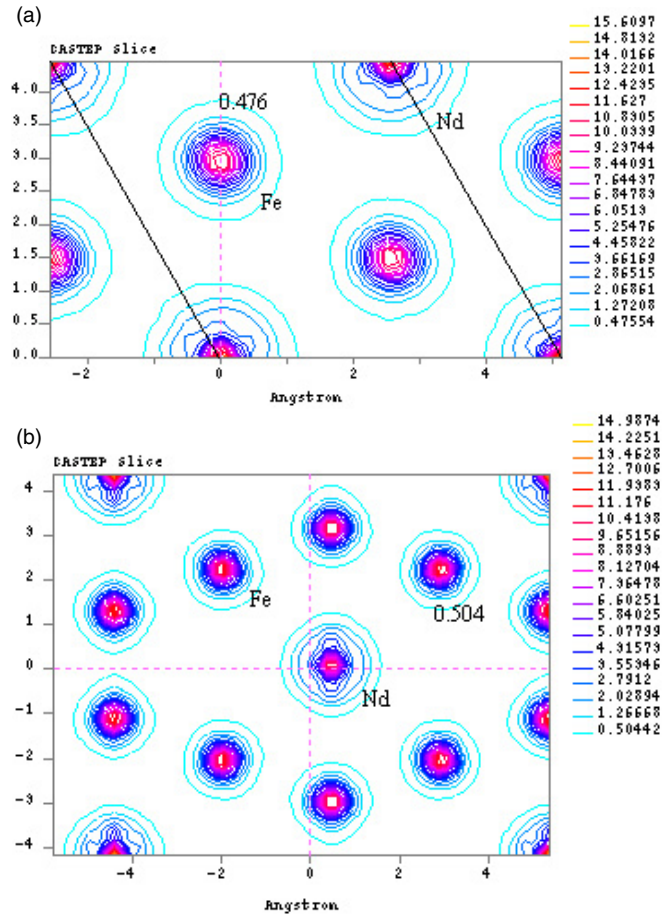

Figure 2. The contour maps of the charge density: (a) on the (0 0 1) plane of $NdFe_5$; (b) on the (1 0 0) plane of Nd_3Fe_{29}. The denoted numbers indicate the numbers of electrons $Å^{-3}$.

(This figure is in colour only in the electronic version)

site preference of ternary additions in Ni_3Al and Fe_3Al [16, 17], phase stability in rare-earth intermetallic compounds [18–23] and so on. It is found finally that the inverted pair potentials are quite reliable for the calculations of the cohesive energy and the structural properties of rare-earth intermetallics; for example, they can predict the phase stability, site preference and lattice constants.

Figure 2 shows the contour maps of charge density in RFe_5 and R_3Fe_{29} which are calculated using the CASTEP software package [24]. In these cases, the main part of the charge density distributions surrounding each atom demonstrates spherical symmetry and does not show evident directionality. This could partly explain why the simple isotropic pair potentials work for these systems. We can thereby simulate the multi-element system with a large cell, e.g. $(R_3(Fe, T)_{29})_{2\times2\times2}$ in this paper, and take the relaxation effect into account, sheering away from the difficulties of quantum mechanics when treating a large cell.

On the other hand, the pair potentials are not universal for any atomistic simulation. The pair potentials cannot, in principle, include the effects of directional bonds. For example, in

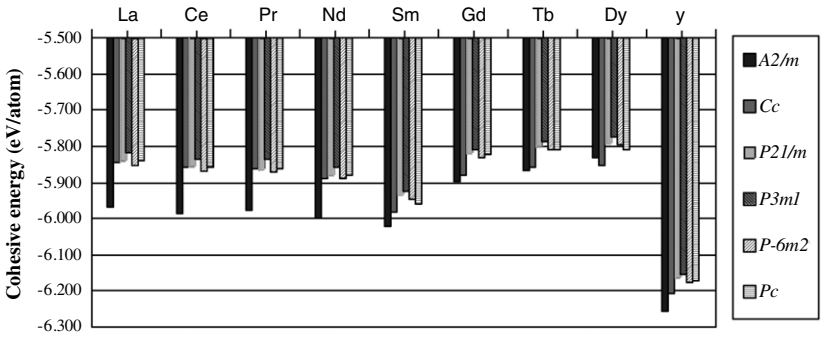

Figure 3. The cohesive energies of different relaxed structures of R_3Fe_{29} compounds.

semiconductors or pure bcc metals, the pair potentials are ineffective to deal with the directional effects. Further, pair potentials are not able to reproduce correctly all elastic constants. There are various Cauchy relations which are not usually fulfilled by the system studied. In these cases many-body terms should be considered.

3. Calculated results for the ternary compounds $R_3(Fe, T)_{29}$

The structures of R_3Fe_{29} and $R_3(Fe, T)_{29}$ have been calculated by the energy minimization process with the conjugate gradient method. The cut-off radius of atomic interactions was taken to be 14 Å. A supercell with 512 atoms has been employed to represent the system.

3.1. Structure

As before a metastable binary structure R_3Fe_{29} is taken at the beginning, which can be obtained from the RFe_5 structure, with the replacement of two-fifths of the R atoms in RFe_5 by Fe–Fe dumbbells [19]. In this procedure we attempt different types of substitutions for rare-earth atoms then let the structure relax under the pair potentials. In the end, we get six kinds of structures which belong to $A2/m$, Cc, $P2_1/m$, $P3m1$, $P\bar{6}m2$ and Pc space groups respectively. The cohesive energies of the R_3Fe_{29} (R = La, Ce, Pr, Nd, Sm, Gd, Tb, Dy, Y) with different space groups are listed in figure 3. It can be seen that the structure with $A2/m$ space group has the lowest cohesive energy except for Dy. In this paper, we only take account of the structure with $A2/m$ space group. Figure 4 shows the calculated x-ray diffraction spectrum of Y_3Fe_{29}, which is very close to the experimental spectrum of $Y_3(Fe, Ti)_{29}$ [25].

3.2. Phase stability

Based on the above R_3Fe_{29} structures and the interatomic potentials ($\Phi_{R-R}(r)$, $\Phi_{Fe-Fe}(r)$, $\Phi_{T-T}(r)$, $\Phi_{R-T}(r)$, $\Phi_{R-Fe}(r)$ and $\Phi_{Fe-T}(r)$), the phase stability of $R_3Fe_{29-x}T_x$ with ternary elements T can be tested. Firstly, a certain number of T atoms are substituted for the Fe atoms at one kind of sites in R_3Fe_{29}. Secondly, the energy minimization procedure is applied to relax the ternary system under interatomic potentials. Thus, the curves of the cohesive energy versus the content of ternary element for each kind of Fe sites can be obtained. The results are shown in figure 5. To avoid the random error, the results are taken as the arithmetic average of 30 stochastic samples. In fact, the fluctuation is very small. It can be seen in figure 5 that

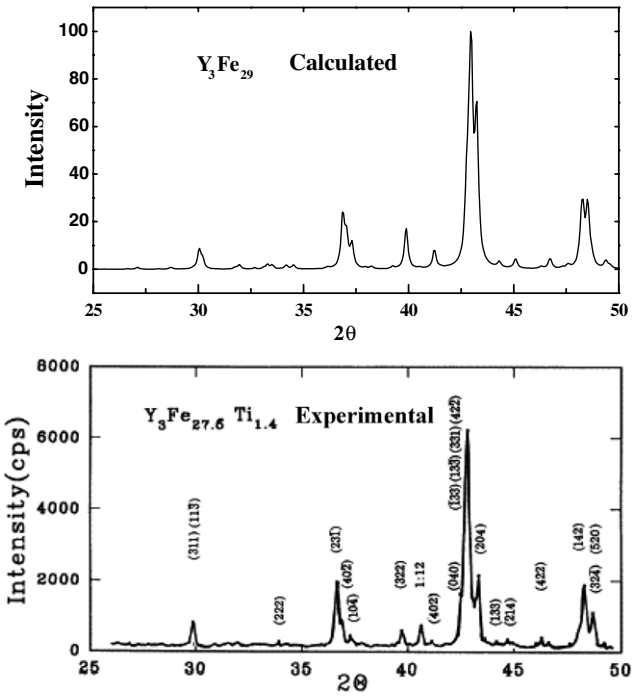

Figure 4. Calculated XRD of Y_3Fe_{29} and experimental results of $Y_3(Fe, Ti)_{29}$.

the cohesive energies decrease obviously with the increasing content of the ternary elements, thus Ta and W atoms can stabilize the system.

3.3. Site preference and tolerance

Comparing the curves shown in figure 5, it is found that the cohesive energies decrease most significantly when T atoms occupy $4i_3$, $4i_4$ and 4g sites. Therefore, the T atoms preferentially occupy the $4i_3$, $4i_4$ and 4g sites, which are in good agreement with the experimental results [26].

It is seen that there is a deviation in the curves of $Gd_3Fe_{29-x}Ta_x$ as shown in figure 5(a); when the content of ternary element $x > 1.9$, the cohesive energy of the preferable 4g sites is higher than that of $8j_1$ and $8j_2$ sites. This does not mean that the element Ta prefers to occupy $8j_1$ or $8j_2$ sites instead of 4g sites. This can be explained by the tolerance. The so-called tolerance is the distance of the atom deviating from the lattice point when identifying the space group of the crystal and the tolerance range indicates the atomic derivation distance, which can be viewed as the error in the process of determining the space group of the compound. In fact, when the ternary element occupies $4i_3$, $4i_4$ and 4g sites the value of tolerance is under 0.6 Å, but for $8j_1$ or $8j_2$ sites, the value of tolerance exceeds 0.8 Å. The large tolerance indicates the instability of the substitution.

The tolerance is shown in figure 6. Note that the tolerance of the three preferential sites is different; the relation of the tolerance values for the three sites is $4i_3 < 4i_4 < 4g$: this indicates the order of site preference of Ta and W in $R_3(Fe, T)_{29}$ is $4i_3$, $4i_4$ and 4g.

It can also be seen in figure 6 that, when $x = 2.0$, the tolerance of the three sites suddenly drops down to 0.01 Å. This is because the Fe atoms at the particular sites are all substituted, and the structure of the system is very symmetric. Hence, in the process of minimization with the conjugate gradient method, the space group of $A2/m$ is easy to keep. We cannot draw a

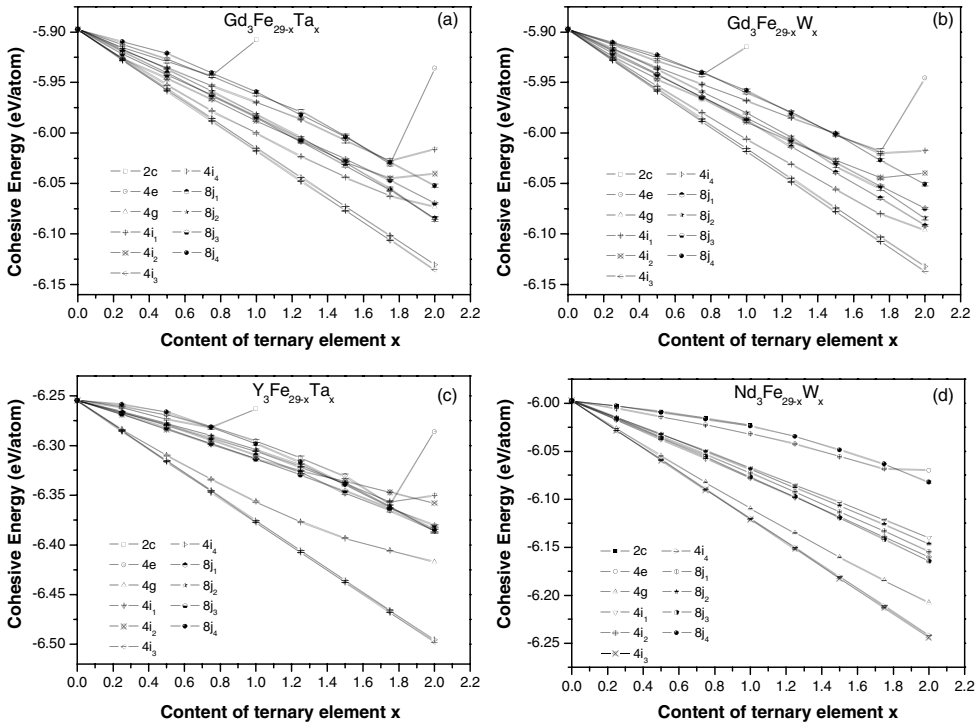

Figure 5. The dependence of cohesive energy on the content of T (T = Ta, W) elements in $R_3Fe_{29-x}T_x$ (R = Gd, Y, Nd).

Table 1. Comparison of lattice constants between the calculated and experimental values [26–28].

	Cell parameters									
Compounds	*a* (Å)	Err. (%)	*b* (Å)	Err. (%)	*c* (Å)	Err. (%)	*β* (deg)	Err. (%)	*V* (Å^3)	Err. (%)
$Gd_3Fe_{28}Ta$ (cal.)	10.582	0.18	8.499	0.01	9.761	0.32	97.14	0.12	871.21	0.14
(Exp.)	10.601		8.498		9.730		97.02		869.96	
$Gd_3Fe_{28.2}W_{0.8}$ (cal.)	10.562	0.18	8.479	0.64	9.748	0.51	97.04	0.19	866.40	0.36
(Exp.)	10.581		8.534		9.699		96.86		869.50	
$Y_3Fe_{28}Ta$ (cal.)	10.600	0.49	8.516	0.47	9.769	1.1	97.14	0.66	874.10	1.89
(Exp.)	10.548		8.476		9.663		97.78		857.81	
$Nd_3Fe_{27.5}W_{1.5}$ (cal.)	10.719	1.01	8.595	0.21	9.852	1.13	97.41	0.68	902.35	2.45
(Exp.)	10.612		8.577		9.742		96.75		880.72	

conclusion that when $x = 2.0$ there exists the most stabilized state, and we can verify this in the reported experimental results [26–28].

3.4. Cell parameters

The calculated cell parameters are listed in table 1. In the calculation the ternary elements were assumed to distribute randomly in the $4i_3$ sites. Comparing the calculated results with the experimental data, it is found that the largest deviation is 1.01% for *a*, 0.64% for *b* and 1.13% for *c*. For the volume of the $R_3(Fe, T)_{29}$ unit cell, the average deviation is 1.21%,

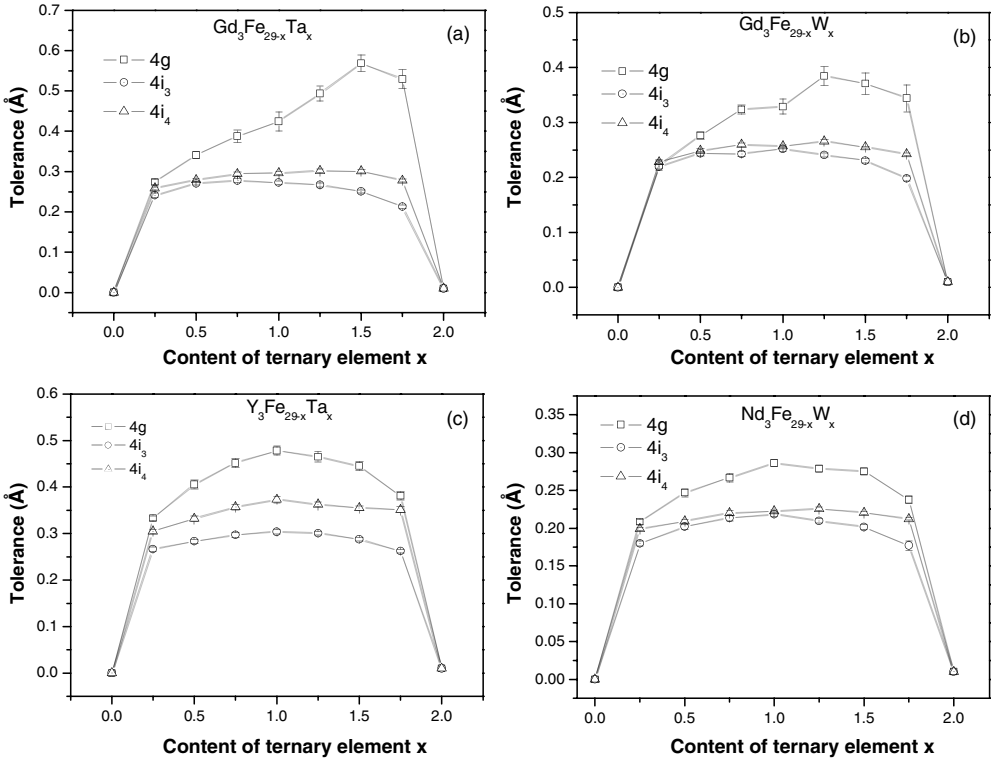

Figure 6. Tolerance of $R_3Fe_{29-x}T_x$ (R = Gd, Y, Nd; T = Ta, W).

Table 2. The MD results of $Y_3Fe_{28}Ta$ and $Nd_3Fe_{27.5}W_{1.5}$.

		Cell parameters					
Compounds	T (K)	a (Å)	b (Å)	c (Å)	Beta (deg.)	Tolerance (Å)	Space group
$Y_3Fe_{28}Ta$	300	10.6058	8.5291	9.7865	97.1354	0.32	$A2/m$
	600	10.6236	8.5433	9.8034	97.1365	0.39	$A2/m$
	800	10.6355	8.5526	9.8151	97.1354	0.39	$A2/m$
	1000	10.6477	8.5620	9.8272	97.1326	0.40	$A2/m$
$Nd_3Fe_{27.5}W_{1.5}$	300	10.7385	8.6310	9.8679	97.4090	0.34	$A2/m$
	600	10.7572	8.6458	9.8851	97.4090	0.43	$A2/m$
	800	10.7696	8.6559	9.8973	97.4125	0.50	$A2/m$
	1000	10.7832	8.6661	9.9084	97.4137	0.50	$A2/m$

and the largest deviation is 2.45%. Figure 7 shows the lattice parameters as a function of ternary elemental content for $Nd_3(Fe_{1-x}W_x)_{29}$. As we just discussed above, the contributions of different kinds of sites are not equal. It can be seen from the curves that when the ternary element occupies the 4g sites the volume of the compound changes to the greatest degree.

3.5. Molecular dynamics simulation

In order to further verify the phase stability of $R_3(Fe_{1-x}, T_x)_{29}$ at different temperatures, the molecular dynamics simulation method is used for the systems of $(Y_3Fe_{28}Ta)_{2\times2\times2}$ and

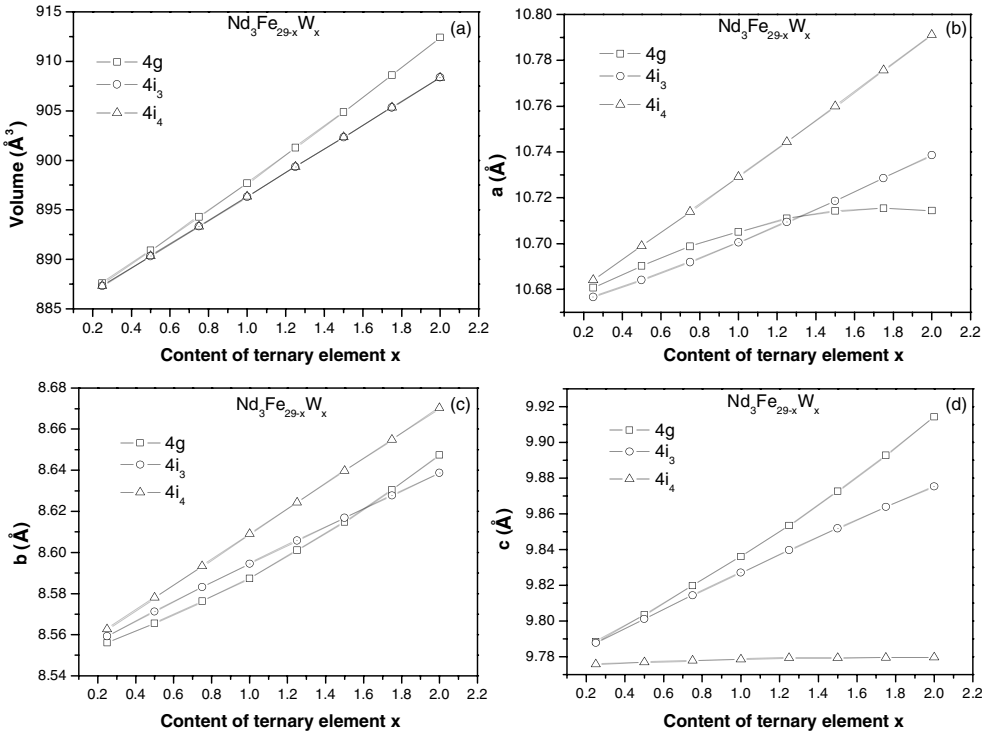

Figure 7. Cell parameters of $Nd_3Fe_{29-x}W_x$ versus the content of ternary element x.

Table 3. Potential and kinetic energies at different temperatures.

	$Y_3Fe_{28}Ta$				$Nd_3Fe_{27.5}W_{1.5}$			
	300 K	600 K	800 K	1000 K	300 K	600 K	800 K	1000 K
E_p (eV/atom)	−6.338	−6.298	−6.271	−6.244	−6.143	−6.103	−6.077	−6.050
E_k (eV/atom)	0.039	0.077	0.103	0.1281	0.039	0.077	0.103	0.128

$(Nd_3Fe_{27.5}W_{1.5})_{2\times2\times2}$. In the calculation the molecular dynamics NPT ensemble is used, with $P = 1$ atm, $t = 0.001$ ps. The molecular dynamics simulation for each of the systems is carried out at temperatures of 300, 600, 800 and 1000 K, respectively. Table 2 shows the values of the cell parameters, tolerance and space group calculated at different temperatures. The most interesting thing is that the space group $A2/m$ can remain in a certain range (tolerance $\leqslant$0.5 Å) and the lattice parameters change very little with increasing temperature. Table 3 shows the potential energy and kinetic energy at the different temperatures. It can be seen from the table that both the values of potential and kinetic energy increase with the increasing temperature, but the contribution of interatomic potentials to the internal energy of the system is much larger than that from thermal motion energy. Therefore, the crystal structure at different temperatures is basically determined by the interatomic pair potentials.

Here, high temperature disturbance embodies the dynamic equilibrium properties at different temperatures. It is reasonable to conclude that the inverted pair potentials are effective in studying not only the characters of the equilibrium state but also the non-equilibrium properties to some extent.

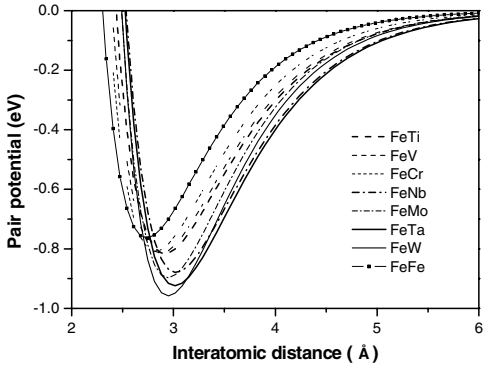

Figure 8. Some Fe–T (T = some 3d, 4d and 5d elements) pair potentials.

4. Discussion and analysis

4.1. Phase stability

The stabilizing effect of the ternary elements can be qualitatively analysed based on the pair potential curves. When ternary elements are involved in the ternary compounds there are six pairs of interatomic potentials in the system, i.e. $\Phi_{R-R}(r)$, $\Phi_{Fe-Fe}(r)$, $\Phi_{T-T}(r)$, $\Phi_{R-T}(r)$, $\Phi_{R-Fe}(r)$ and $\Phi_{Fe-T}(r)$. These potentials show different effects on the system in different situations. When a small number of ternary atoms replace the Fe atoms, the atoms surrounding each ternary atom are mostly Fe atoms. The rare-earth atoms are not their own nearest-neighbour atoms, and the occasions where two T atoms are the nearest neighbours are truly rare. Therefore, the difference between $\Phi_{Fe-T}(r)$ and $\Phi_{Fe-Fe}(r)$ becomes the dominating factor that induces the energy difference between before and after substitution, and the role of $\Phi_{R-R}(r)$ and $\Phi_{T-T}(r)$ can be ignored. If $\Phi_{Fe-T}(r) < \Phi_{Fe-Fe}(r)$, the ternary element will show the effect of stabilizing the structure. For example, with $Gd_3(Fe, Ta)_{29}$, as can be seen in figure 1, $\Phi_{Fe-Ta}(r)$ intersects $\Phi_{Fe-Fe}(r)$ at 2.74 Å. When the interatomic distance is $r > 2.74$ Å, we have $\Phi_{Fe-Ta}(r) < \Phi_{Fe-Fe}(r)$. This means Ta atoms substituting for Fe will result in the decrease of the system cohesive energy, and Ta can stabilize the system.

When the amount of the ternary element increases, the T atoms will have more opportunity to get close to other T atoms or rare-earth atoms and $\Phi_{T-T}(r)$ or $\Phi_{T-R}(r)$ should be involved. For the system of $Gd_3Fe_{29-x}Ta_x$, $\Phi_{Gd-Ta}(r)$ intersects $\Phi_{Gd-Fe}(r)$ at 3.12 Å, and $\Phi_{Ta-Ta}(r)$ intersects $\Phi_{Fe-Fe}(r)$ at 2.94 Å. If $r < 3.12$ Å we have $\Phi_{Gd-Ta}(r) > \Phi_{Gd-Fe}(r)$, and if $r < 2.94$ Å we have $\Phi_{Ta-Ta}(r) > \Phi_{Fe-Fe}(r)$. When the ternary element atoms are excessive, the average distance between the R atom and T atom or between the T atom and T atom decreases; then the total energy will increase, which causes a structural instability.

4.2. Solubility

The solubility can also be qualitatively analysed based on the pair potential analysis. Figure 8 shows the pair potentials of some $\Phi_{Fe-T}(r)$ (T = certain 3d, 4d or 5d stabilizing elements). It can be seen from the figure that the minima of the curves for $\Phi_{Fe-T}(r)$ are lower compared with that of $\Phi_{Fe-Fe}(r)$, and this may be one of the main reasons why certain 3d, 4d and 5d elements T (T = Ti, V, Cr, Nb, Mo, Ta, W) can stabilize the $R_3(Fe, T)_{29}$ compounds. When 3d elements (T = Ti, V, Cr) act as stabilizing elements, the minimum of each curve $\Phi_{Fe-T}(r)$ is adjacent, but that of $\Phi_{Fe-T}(r)$ with 4d elements (T = Nb, Mo) is lower than that of 3d, and $\Phi_{Fe-T}(r)$

with 5d elements (T = Ta, W) is lower than that of 3d and 4d elements. Therefore, different contents are needed to stabilize $R_3(Fe_{1-x}, T_x)_{29}$ for the different transitional elements, and in order to stabilize the system more T element in 3d families is needed compared with T element in 5d families. But we cannot get a very stabilizing compound by adding excessive 5d element. This is because in this process the atom displacements and crystal distortions become more and more obvious and it is difficult to maintain the original $A2/m$ structure. This can be seen in the tolerance analysis in the previous section. With the same ternary content x, the value of tolerance of a 5d element is much larger than that of a 3d element [19]. Consequently, the range of solubility of 5d elements is narrower than that of 3d elements. It has been found that the content x of 5d ternary elements needed for stabilizing the 3:29 structure is not more than 1.5 [26–28].

For the synthesized compounds with $Nd_3(Fe, Ti)_{29}$ structure, the non-magnetic elements usually act as stabilizing selement, and the minimum content needed to stabilize the system varies for the different ternary elements. The system needs a smaller amount of certain 5d elements than of 3d elements for the stabilized state and the loss of the magnetic properties will be small.

5. Conclusion

The interatomic potentials related to R (rare earth Nd, Gd and Y) and transition elements (Fe and 5d elements Ta, W) have been obtained in terms of the lattice inversion method. Using these potentials the behaviour of the 5d transition elements Ta, W acting as the ternary elements in $R_3(Fe, T)_{29}$ compounds have been studied. It is found that both Ta and W can stabilize the ternary compounds well even though the atom is heavier and the atomic radius is larger than 3d or 4d transition elements. The two ternary elements prefer to occupy the $4i_3$, $4i_4$, and 4g sites, but these sites are still different for attracting the ternary elements Ta and W. The preferential order of Ta and W basically is $4i_3$, $4i_4$ and 4g. The calculated cell parameters of $Gd_3Fe_{28}Ta$, $Gd_3Fe_{28.2}W_{0.8}$, $Y_3Fe_{28}Ta$ and $Nd_3Fe_{27.5}W_{1.5}$ are in good agreement with the experiments. In order to further examine the structural stability at different temperatures, molecular dynamics simulations have been employed, and the results show that within the range of tolerance < 0.5 Å the relaxed structure of the compounds can remain in the space group of $A2/m$. Based on the interatomic potential curves, the phase stability and the solubility are qualitatively analysed. It is found that the solubility of 5d elements is narrower than that of 3d or 4d elements. The lower solubility means fewer non-magnetic ternary atoms are added, which induces more magnetic Fe atoms to remain. Therefore, the 5d elements Ta and W will benefit the magnetic properties of the materials compared with the 3:29 materials with 3d or 4d ternary elements.

Acknowledgments

The authors would like to thank Professor F M Yang at the Institute of Physics, Chinese Academy of Science, for stimulating discussions. This work is supported by National 973 Project TG2000067101 and TG2000067106 of China.

References

[1] Buschow K H J 1980 *Ferromagnetic Materials* vol 1, ed E P Wohlfarth (Amsterdam: North-Holland) p 297
Buschow K H J 1980 *Ferromagnetic Materials* vol 4, ed E P Wohlfarth (Amsterdam: North-Holland) p 1
[2] Collocott S J, Day R K, Dunlop J B and Davis R L 1992 *Proc. 7th Int. Symp. on Magnetic Anisotropy and Coercivity in Rare Earth–Transition Alloys (Canberra)* p 437
[3] Li H S, Cadogan J M, Bowden G J, Xu J M, Dou S X and Liu H K 1994 *J. Appl. Phys.* **75** 7120

[4] Hu Z and Yelon W B 1994 *J. Appl. Phys.* **76** 6147
[5] Kalogirou O, Psycharis V, Saettas L and Niarchos D 1995 *J. Magn. Magn. Mater.* **146** 335–45
[6] Cadogan J M, Li H S, Margarian A, Dunlop J B, Ryan D H, Collocott S J and Davis R L 1994 *J. Appl. Phys.* **76** 6138
[7] Han X F, Yang F M, Pan H G, Wang Y G, Wang J L, Liu H L, Tang N, Rao R W and Li H S 1997 *J. Appl. Phys.* **81** 7450
[8] Pan H G, Yang F M, Chen C P, Han X F, Tang N and Wang Q D 1996 *J. Magn. Magn. Mater.* **161** 177
[9] Chen N X, Chen Z D and Wei Y C 1997 *Phys. Rev.* E **55** R5
[10] Chen N X and Ren G B 1992 *Phys. Rev.* B **45** 8177
[11] Chen N X, Ge X J, Zhang W Q and Zhu F W 1998 *Phys. Rev.* B **57** 14203
[12] Maddox J 1990 *Nature* **344** 377
[13] Zhang W Q, Xie Q, Ge X J and Chen N X 1997 *J. Appl. Phys.* **82** 578d
[14] Li M and Chen N X 1995 *Phys. Rev.* B **52** 997–1003
[15] Liu S J, Duan S Q and Ma B K 1998 *Phys. Rev.* B **58** 9705
[16] Shen J, Wang Y, Chen N X and Wu Y 2000 *Prog. Natl Sci.* **10** 457
[17] Ni X D, Chen N X and Shen J 2001 *J. Mater. Res.* **16** 344
[18] Chen N X, Shen J and Su X P 2001 *J. Phys.: Condens. Matter* **13** 2727–36
[19] Cao L Z, Shen J and Chen N X 2002 *J. Alloys Compounds* **336** 18–28
[20] Chen N X, Shen J and Wang X L 2003 *J. Alloys Compounds* **359** 91–8
[21] Hao S Q and Chen N X 2002 *Phys. Lett.* A **297** 110–20
[22] Hao S Q, Chen N X and Shen J 2002 *J. Alloys Compounds* **343** 53
[23] Chang H, Chen N X, Liang J K and Rao G H 2002 *J. Phys.: Condens. Matter* **14** 1–12
[24] Payne M C, Teter M P, Allan D C, Arias T A and Joannopoulos L D 1992 *Rev. Mod. Phys.* **64** 1045
[25] Yang F M, Han X F, de Boer F R and Li H S 1997 *J. Phys.: Condens. Matter* **9** 1339–46
[26] Liu Q L, Rao G H, Liang J K and Shen B G 2000 *J. Appl. Phys.* **88** 4241
[27] Skolozdra R V, Fruchart D, Kalychak M and Bououdina M 2000 *J. Alloys Compounds* **296** 258–64
[28] Sánchez L1 J L, Santana Gil A D, Matutes Aquino J and Torres-Garibay C 2000 *J. Alloys Compounds* **313** L15–8